Far field of gratings with rough strips

Luis Miguel Sanchez-Brea,* Francisco Jose Torcal-Milla, and Eusebio Bernabeu

Applied Optics Complutense Group, Optics Department, Universidad Complutense de Madrid, Facultad de Ciencias Físicas, Ciudad Universitaria s.n., 28040, Madrid, Spain
**Corresponding author: sanchezbrea@fis.ucm.es*

Received October 4, 2007; revised January 24, 2008; accepted January 26, 2008;
posted January 29, 2008 (Doc. ID 88270); published March 4, 2008

In this work, we analyze the far-field pattern produced by a grating made of strips with two different random roughness levels. The efficiency and shape of the diffraction orders is obtained, which are shown to depend on the statistical properties of roughness. We assume for the calculations that the grating can be used in a mobile mechanical system. A preliminary experimental approach which partially corroborates the theoretical results is also performed. © 2008 Optical Society of America

OCIS codes: 050.0050, 050.2770.

1. INTRODUCTION

When a light beam impinges into a diffraction grating, it is divided into several waves with different directions of propagation, according to the well-known grating equation [1,2]. This characteristics of diffraction gratings make them one of the most important optical elements, and they have contributed to the advance of numerous branches of science such as chemistry, biology, astrophysics, photonics, and mechanical engineering. Diffraction gratings can be found in such diverse devices as spectrometers, colorimeters, nanopositioners, and telescopes [3]. Although the study of diffraction gratings dates to the late 18th century they are still a subject of research [4,5].

Ordinary gratings act on the amplitude and/or the phase of a wavefront, and they can work in transmission or reflection configurations [6,7]. Other kinds of gratings are possible, such as polarization gratings, in which a periodic modulation of the state of polarization is produced [8–10]. Another unexplored possibility is to periodically modify the microscopic characteristics of the grating, producing strips with different roughness levels. Gratings with roughness can be found, for example, when the substrate is metallic as in steel tape gratings, which are used in optical metrology. Steel tape gratings have been analyzed under a high roughness approach [11,12]. Rough slits scatter light in all directions, and only a small portion of this scattered light reaches the photodetectors. Steel tape gratings behave as if they were amplitude gratings.

In the present work, we analyze a grating with different roughness levels under a more general approach, since we consider any arbitrary roughness level. In fact, surfaces always present a certain roughness. The characteristics of the far-field diffraction pattern are determined in terms of the statistical properties of roughness. For example, the mutual intensity and the efficiency of the diffraction orders are obtained, which are shown to depend on the roughness parameters. The intensity of the far-field diffraction pattern is also obtained for high and low roughness limits, theoretically justifying the assumptions made in previous works. Preliminary experimental results for the case of a transmission grating where one of the levels is rough are also obtained, corroborating the validity of the proposed framework.

2. GRATINGS WITH ROUGH STRIPS

Let us consider a grating with period p formed by strips with two different roughness levels. Without loss of generality, a transmission grating made of a dielectric material with refraction index n will be considered. Reflection gratings can be studied under a similar method. A three-dimensional approach will be analyzed, where x is the axis transverse to the strips, y is the axis parallel to the strips, and z is the axis perpendicular to the grating. One of the levels of the grating presents a constant height $\zeta_0 = 0$, and the other level presents a rough surface with a random topography $\zeta(x,y)$ whose average height is null, $\langle \zeta(x,y) \rangle = 0$; see Fig. 1(a). Let us consider the thin element approach to calculate the phase delay produced by the grating [13]. Then, the transmittance in the strips with a rough surface may be expressed as $t(x,y) = \exp[ik(n-1)\zeta(x,y)]$, where $k = 2\pi/\lambda$ and λ is the wavelength of the incident light field, which is assumed to be a monochromatic plane wave.

Mathematically, this grating can be described as a sum of two amplitude binary gratings with period p (average amplitude levels 0 and 1). The first grating is

$$G_1(x) = \sum_l a_l \exp(iqlx), \tag{1}$$

where $q = 2\pi/p$. The Fourier coefficients of grating $G_1(x)$ are $a_l = \kappa\,\mathrm{sinc}(l\pi\kappa)$, with $\kappa = \alpha/p$, as defined in Fig. 1(b). This grating presents a rough surface, thus the transmittance for the rough strips is $G(x,y) = t(x,y)G_1(x)$.

The second grating is formed by slits with a constant height $G_2(x) = 1 - G_1(x)$, Fig. 1(c). The sum of these two amplitude gratings,

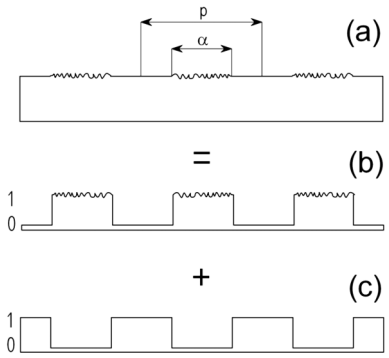

Fig. 1. Diffraction grating formed as a sum of two amplitude gratings. One of them presents a rough surface.

$$T(x,y) = 1 - G_1(x)[1 - t(x,y)], \tag{2}$$

describes the whole structure, which acts stochastically on the phase of the incident wave. When roughness is null, then $t(x,y)=1$ and the grating disappears, as the transmittance is $T(x,y)=1$.

To describe the statistical properties of the rough strips, we will assume a normal distribution in heights $w(z)=\exp(-z^2/2\sigma^2)/\sqrt{2\pi}\sigma$, where $z=\zeta(x,y)$ and σ is the standard deviation. The average scattering coefficient, according to Beckmann and Spizzichino [14], is

$$\langle t(x,y)\rangle = \int \mathrm{d}z w(z)\exp[ik(n-1)z] = \exp(-g/2),$$

where $g=[k\sigma(n-1)]^2$.

Let us consider that a plane wave in normal incidence with amplitude A_0 illuminates the grating. The amplitude just after the grating is $U_1(x,y)=A_0T(x,y)$. From here, we will assume that the random process that represents the fields produced by a hypothetical ensemble of diffusers is stationary and, therefore, the amplitude correlation of the speckle field,

$$J(x,x',y,y') = \langle U_1(x,y)U_1^*(x',y')\rangle = |A_0|^2\langle T(x,y)T^*(x',y')\rangle,$$

gives

$$\frac{J(x,x',y,y')}{|A_0|^2} = 1 + [G_1(x) + G_1^*(x')](\langle t(x,y)\rangle - 1) + G_1(x)G_1^*(x')[\langle t(x,y)t^*(x',y')\rangle - 2\langle t(x,y)\rangle + 1], \tag{3}$$

where we have considered that $\langle t^*(x',y')\rangle=\langle t(x,y)\rangle = \exp(-g/2)$, and the angle brackets represent the average over the ideal ensemble of transmittance coefficients.

More assumptions about the statistical properties of the topography $\zeta(x,y)$ are required. We will consider that the two-dimensional distribution of heights $z_1=\zeta_1(x,y)$ and $z_2=\zeta_2(x',y')$ at two different points (x,y) and (x',y') with mean values zero and variances σ^2, is

$$w(z_1,z_2) = \frac{1}{2\pi\sigma\sqrt{1-C(\tau,\eta)^2}}\exp\left[-\frac{z_1^2 - 2C(\tau,\eta)z_1z_2 + z_2^2}{2\sigma^2(1-C(\tau,\eta)^2)}\right], \tag{4}$$

where the autocorrelation coefficient is Gaussian $C(\tau,\eta)=\langle\zeta_1\zeta_2\rangle/\langle\zeta_1^2\rangle=\exp[-(\tau^2+\eta^2)/T_0^2]$, $\tau=x-x'$, $\eta=y-y'$, and T_0 is the correlation distance. As a result, the characteristic function of this two-dimensional distribution may be expressed as [14]

$$\langle t(x_1,y_1)t^*(x'_1,y'_1)\rangle = \exp\{-g[1-C(\tau,\eta)]\} = e^{-g}\sum_{m=0}^{\infty}\frac{g^m}{m!}e^{-m(\tau^2+\eta^2)/T_0^2}. \tag{5}$$

Inserting Eq. (5) into Eq. (3), we obtain the mutual intensity function [15]

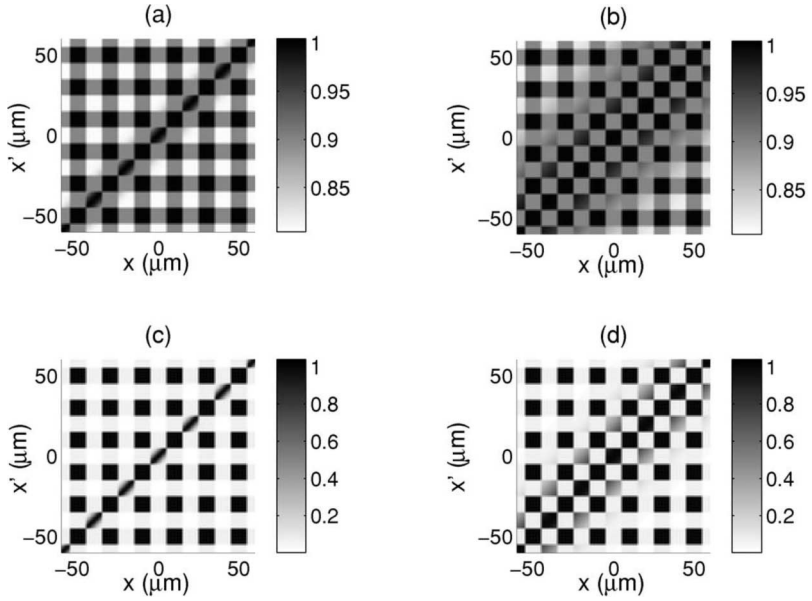

Fig. 2. Mutual intensity $J(x,x',0,0)$ just after the diffraction grating when $p=20$ μm, $\lambda=0.68$ μm, $\kappa=0.5$, $R_x=0.1$ mm, $R_y=0.1$ mm, and $n=1.5$ for four cases: (a) $\sigma=0.1$ μm, $T_0=10$ μm; (b) $\sigma=0.1$ μm, $T_0=50$ μm; (c) $\sigma=0.5$ μm, $T_0=10$ μm; and (d) $\sigma=0.5$ μm, $T_0=50$ μm.

$$\frac{J(x,x',y,y')}{|A_0|^2} = 1 - [G_1(x) + G_1^*(x')][1 - \exp(-g/2)] + G_1(x)G_1^*(x')\left\{[1 - \exp(-g/2)]^2 + e^{-g}\sum_{m=1}^{\infty}\frac{g^m}{m!}e^{-m(\tau^2+\eta^2)/T_0^2}\right\}. \quad (6)$$

In Figure 2, the mutual intensity function $J(x,x',0,0)$ just after the diffraction grating is represented for several cases with different roughness parameters. The average intensity distribution $\langle I(x,y)\rangle$ just after the grating is obtained from the mutual intensity [15] $\langle I(x,y)\rangle = J(x,x,y,y)$. This corresponds to the diagonal of the mutual intensity function, and in all cases, it is a constant $I(x,x',y,y') = |A_0|^2$.

3. INTENSITY DISTRIBUTION AT THE FAR FIELD

The amplitude $U_2(x_2,y_2)$ at the far field can be determined using the Fraunhofer approach. Let us consider now that the grating presents a finite size in length and width. Then the amplitude just after the grating is

$$U_1(x,y) = A_0 T(x,y)\prod(x/R_x)\prod(y/R_y), \quad (7)$$

where $\Pi(x)$ is the rectangle function

$$\prod(x/R) = \begin{cases} 1 & |x| \le R/2 \\ 0 & |x| > R/2 \end{cases}. \quad (8)$$

The amplitude U_2 is proportional to the spatial Fourier transform of the near field:

$$U_2(x_2,y_2) = \frac{e^{ik[z+(x_2^2+y_2^2)/2z]}}{i\lambda z}\int\int U_1(x_1,y_1) \times \exp\left[\frac{-ik}{z}(x_1x_2 + y_1y_2)\right]dx_1dy_1, \quad (9)$$

where (x_2,y_2) is the location of the observation plane. Because of the stochastic nature of the grating, in our case we cannot explicitly determine the amplitude at a distance z from the grating, but we can write the mutual intensity function as

$$J(x_2,x'_2,y_2,y'_2) = K\int_{-R_y/2}^{R_y/2}\int_{-R_y/2}^{R_y/2}\int_{-R_x/2}^{R_x/2}\int_{-R_x/2}^{R_x/2} \times J(x_1,x'_1,y_1,y'_1)e^{ik/z(x'_2x'_1+y'_2y'_1-x_2x_1-y_2y_1)} \times dx_1dx'_1dy_1dy'_1, \quad (10)$$

where we have included the rectangle functions in the integration limits, and $K = \exp[ik/2z(x_2^2 - x_2'^2 + y_2^2 - y_2'^2)]/(\lambda z)^2$. Assuming that $R_x, R_y \gg T_0, p, \lambda$, then the result of this integral is

$$\frac{J(\theta_x,\theta'_x,\theta_y,\theta'_y)}{K|A_0|^2R_x^2R_y^2} \approx \operatorname{sinc}\left(\frac{kR_y}{2}\theta_y\right)\operatorname{sinc}\left(\frac{kR_y}{2}\theta'_y\right)\left\{\operatorname{sinc}\left(\frac{kR_x}{2}\theta_x\right)\operatorname{sinc}\left(\frac{kR_x}{2}\theta'_x\right) + (e^{-g/2}-1) \times \operatorname{sinc}\left(\frac{kR_x}{2}\theta'_x\right)\sum_l a_l\operatorname{sinc}\left[\frac{R_x}{2}(k\theta_x - lq)\right] + (e^{-g/2}-1)\operatorname{sinc}\left(\frac{kR_x}{2}\theta_x\right)\sum_{l'} a_{l'}^*\operatorname{sinc}\left[\frac{R_x}{2}(k\theta'_x - l'q)\right] + (1-e^{-g/2})^2\sum_{l,l'} a_la_{l'}^*\operatorname{sinc}\left[\frac{R_x}{2}(k\theta_x - lq)\right]\operatorname{sinc}\left[\frac{R_x}{2}(k\theta'_x - l'q)\right]\right\} + 4\frac{T_0^2}{R_xR_y}e^{-g}\operatorname{sinc}\left[\frac{kR_y}{2}(\theta'_y - \theta_y)\right]\sum_{l,l'} a_la_{l'}^*\operatorname{sinc}\left\{\frac{R_x}{2}[k(\theta'_x - \theta_x) - (l-l')q]\right\} \times \sum_{m=1}\frac{m^2g^m}{m!}\left[\frac{1}{m^2 + (kT_0\theta_y)^2} + \frac{1}{m^2 + (kT_0\theta'_y)^2}\right]\left[\frac{1}{m^2 + T_0^2(k\theta_y - lq)^2} + \frac{1}{m^2 + T_0^2(k\theta'_y - l'q)^2}\right], \quad (11)$$

where we have written the mutual intensity function in angular coordinates $\theta_x = x_2/z$, $\theta'_x = x'_2/z$, $\theta_y = y_2/z$, $\theta'_y = y'_2/z$. Then, the average intensity of the speckle pattern at the far field $\langle I(\theta_x,\theta_y)\rangle = J(\theta_x,\theta_x,\theta_y,\theta_y)$, is

$$\overline{\langle I(\theta_x,\theta_y)\rangle} = \operatorname{sinc}^2\left(\frac{kR_y}{2}\theta_y\right) \times \left\{\operatorname{sinc}^2\left(\frac{kR_x}{2}\theta_x\right) + 2(e^{-g/2}-1)\operatorname{sinc}\left(\frac{kR_x}{2}\theta_x\right)\sum_l \operatorname{Re}(a_l)\operatorname{sinc}\left[\frac{R_x}{2}(k\theta_x - lq)\right] + (1-e^{-g/2})^2\sum_{l,l'} a_la_{l'}^*\operatorname{sinc}\left[\frac{R_x}{2}(k\theta_x - lq)\right]\operatorname{sinc}\left[\frac{R_x}{2}(k\theta_x - l'q)\right]\right\} + 8\frac{T_0^2}{R_xR_y}e^{-g}\sum_{l,l'} a_la_{l'}^*\operatorname{sinc}\left[\frac{R_x}{2}(l-l')q\right]\frac{1}{m^2 + (kT_0\theta_y)^2}\sum_{m=1}\frac{m^2g^m}{m!}\left[\frac{1}{m^2 + T_0^2(k\theta_x - lq)^2} + \frac{1}{m^2 + T_0^2(k\theta_x - l'q)^2}\right], \quad (12)$$

where $\overline{\langle I(\theta_x,\theta_y)\rangle}=\langle I(\theta_x,\theta_y)\rangle(\lambda z)^2/(|A_0|^2R_x^2R_y^2)$.

Since we have assumed that $R_x,R_y \gg \lambda,p$, the sinc functions are all very narrow, and they do not overlap unless their arguments are equal. As a consequence, the only term that survives in the first summation is that with $l=0$, and in the second and third double summations only those terms with $l=l'$. Then the intensity simplifies to

$$\overline{\langle I(\theta_x,\theta_y)\rangle} = \mathrm{sinc}^2\left(\frac{kR_y}{2}\theta_y\right)\left\{[1+2\,\mathrm{Re}(a_0)(e^{-g/2}-1)]\times\mathrm{sinc}^2\left(\frac{kR_x}{2}\theta_x\right)+(1-e^{-g/2})^2\sum_l |a_l|^2\times\mathrm{sinc}^2\left[\frac{R_x}{2}(k\theta_x-lq)\right]\right\} + 16\frac{T_0^2}{R_xR_y}e^{-g}\sum_{m=1}\frac{g^m}{m!}\frac{m^2}{m^2+(kT_0\theta_y)^2}\times\sum_l\frac{|a_l|^2}{m^2+T_0^2(k\theta_x-lq)^2}. \quad (13)$$

The average intensity distribution can be interpreted as that obtained with two diffraction gratings. The first summation is equivalent to an amplitude grating with Fourier coefficients $(1-e^{-g/2})a_l$. The second summation can also be seen as a diffraction grating since light is split into several beams with directions $\theta_l=l\lambda/p$. However, the diffraction orders are produced by a scattering process. The resulting intensity of a given diffraction order l is

$$\overline{\langle I_l(\theta_x,\theta_y)\rangle} = \mathrm{sinc}^2\left(\frac{kR_y}{2}\theta_y\right)\left\{h_0+(1-e^{-g/2})^2|a_l|^2\times\mathrm{sinc}^2\left[\frac{R_x}{2}(k\theta_x-lq)\right]\right\}+16\frac{T_0^2}{R_xR_y}e^{-g}\times\sum_{m=1}\frac{g^m}{m!}\frac{m^2}{m^2+(kT_0\theta_y)^2}\frac{|a_l|^2}{m^2+T_0^2(k\theta_x-lq)^2}, \quad (14)$$

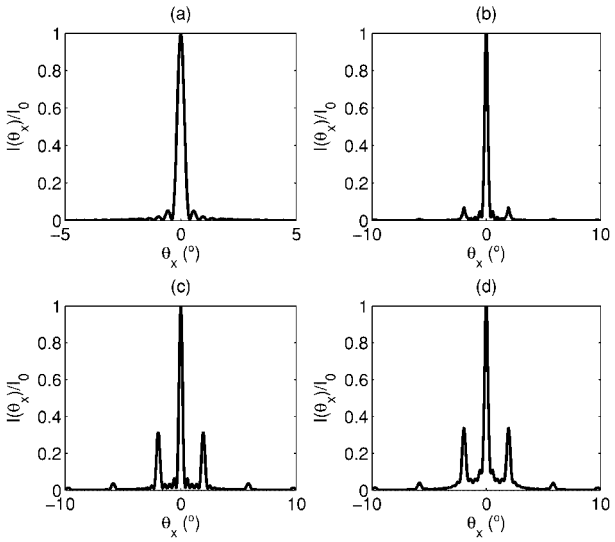

Fig. 3. Intensity at the far field for the situations depicted in Fig. 2.

where $h_0=[1+2\mathrm{Re}(a_0)(e^{-g/2}-1)]\mathrm{sinc}^2\left(\frac{kR_x}{2}\theta_x\right)$ when $l=0$, and $h_0=0$ for the rest of the diffraction orders.

In Figure 3, the average intensity distribution at the far field is shown for different roughness parameters. In all cases, a number of diffraction orders are obtained showing that the grating proposed in Eq. (2) acts as a diffraction grating owing only to its roughness. The height and shape of the diffraction orders depend on the roughness parameters. Using Eq. (14) we can determine the efficiency of the different diffraction orders, which is defined as the ratio between the power of a diffraction order with respect to the total power. Then it can be computed as

$$\eta_l = \frac{\int \overline{\langle I_l(\theta_x,\theta_y)\rangle}\,\mathrm{d}\theta_x\mathrm{d}\theta_y}{\int\sum_l \overline{\langle I_l(\theta_x,\theta_y)\rangle}\,\mathrm{d}\theta_x\mathrm{d}\theta_y}. \quad (15)$$

These integrals cannot be analytically computed, but numerical results can be obtained. Next, we will analyze the efficiency of the diffraction orders for some examples with slight and high roughness limits.

Roughness is slight when $\sigma \ll \lambda$ and as a consequence $g \ll 1$. Performing a linear series expansion in g, the average intensity distribution in the far-field results is

$$\overline{\langle I(\theta_x,\theta_y)\rangle} = \mathrm{sinc}^2\left(\frac{1}{2}kR_x\theta_x\right)\mathrm{sinc}^2\left(\frac{1}{2}kR_y\theta_y\right)[1-g\mathrm{Re}(a_0)] + \frac{16gT_0^2}{R_xR_y(1+k^2T_0^2\theta_y^2)}\sum_l\frac{|a_l|^2}{1+T_0^2(k\theta_x-lq)^2}. \quad (16)$$

In this case, the diffraction orders are produced by a weak scattering process owing to roughness, and the average intensity distribution follows a Lorentz distribution. The width of the diffraction peaks is $\omega_l=\lambda/2\pi T$, which is independent of the diffraction order. The mean intensity of the diffraction peaks is low since it is proportional to T_0^2/R_xR_y, and we have assumed that $R_x,R_y \gg T_0$. As an example, in Figs. 3(a) and 3(b) the intensity at the far field for two cases of slight roughness is shown. Using Eq. (15) we have computed the efficiency of the diffraction orders

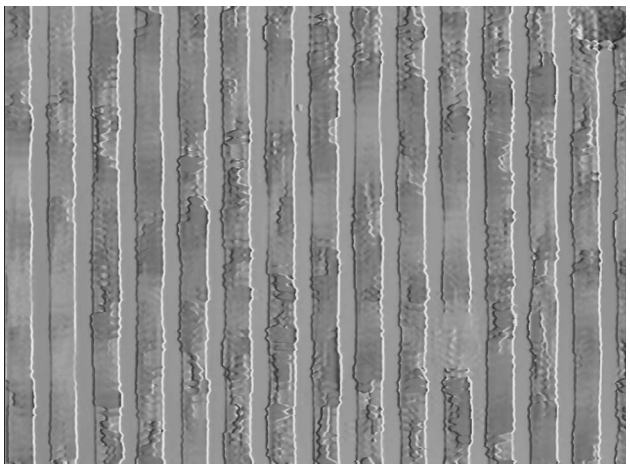

Fig. 4. Confocal microscopy image of the grating used in the experiment.

for these two examples, which results in $\eta_0=0.9693$, $\eta_1=\eta_{-1}=0.015$, and $\eta_3=\eta_{-3}=0.003$ when $\sigma=0.1$ μm and $T_0=10$ μm, and $\eta_0=0.863$, $\eta_1=\eta_{-1}=0.059$, and $\eta_3=\eta_{-3}=0.006$ when $\sigma=0.1$ μm and $T_0=50$ μm. We can see that the efficiency of the diffraction orders other than the zeroth order is quite low for this slight roughness limit.

Obviously, when roughness is null, $g=0$, the intensity distribution,

$$\overline{\langle I(\theta_x,\theta_y)\rangle}=|A_0|^2\frac{R_x^2R_y^2}{(\lambda z)^2}\mathrm{sinc}^2\left(\frac{1}{2}kR_x\theta_x\right)\mathrm{sinc}^2\left(\frac{1}{2}kR_y\theta_y\right), \tag{17}$$

shows that there exists no diffraction grating, but the intensity distribution is produced by the diffraction of a rectangle whose size is equal to the grating size.

For the case of high roughness, $g\gg 1$, the average intensity distribution results is

$$\begin{aligned}\overline{\langle I(\theta_x,\theta_y)\rangle}=&\mathrm{sinc}^2\left(\frac{1}{2}kR_y\theta_y\right)\left\{[1-2\mathrm{Re}(a_0)]\mathrm{sinc}^2\left(\frac{1}{2}kR_x\theta_x\right)\right.\\&\left.+\sum_l|a_l|^2\mathrm{sinc}^2\left[\frac{1}{2}R_x(lq-k\theta_x)\right]\right\}\\&+\frac{16T_0^2}{R_xR_y(1+k^2T_0^2\theta_y^2)}\sum_l\frac{|a_l|^2}{1+T_0^2(lq-k\theta_x)^2}.\end{aligned} \tag{18}$$

The first summation corresponds to the intensity distribution of a binary amplitude diffraction grating whose Fourier coefficients a_l are those of the grating $G_1(x)$. The second summation corresponds to Lorentz distributions produced by scattering and centered at $\theta_x=lq/k$, that is, at the location of the diffraction peaks. The mean intensity of these "halos" is much smaller than that of the peaks determined by the first summation. In Figs. 3(c) and 3(d) the intensity at the far field is shown for two cases of high roughness.

The average intensity distribution can be interpreted in the following way. Light that passes through the nonrough strips interferes as if the strips were just an amplitude grating. Light that passes through the rough strips is scattered in all directions forming in the far field the halos of light around the diffraction peaks. The results obtained with this high roughness limit explain the experimental assumptions performed in [11], where a steel tape grating was shown to behave as an amplitude grating. The efficiency for the examples of Figs. 3(c) and 3(d) results in $\eta_0=0.577$, $\eta_1=\eta_{-1}=0.183$, and $\eta_3=\eta_{-3}=0.020$ when $\sigma=0.5$ μm and $T_0=10$ μm, and $\eta_0=0.556$, $\eta_1=\eta_{-1}=0.193$, and $\eta_3=\eta_{-3}=0.021$ when $\sigma=0.5$ μm and $T_0=50$ μm. The efficiency of the diffraction orders is much higher than in the case of slight roughness.

4. EXPERIMENTAL APPROACH

To confirm the validity of the theoretical model, we have manufactured a grating similar to that proposed in Fig. 1, and we have measured its behavior at the far field. We used a chromium on-glass grating with a period of $p=20$ μm. First we applied a glass etching liquid to the grating for a short time (20 s) which produced a rough surface at the glass zones. Then the chromium was removed with a chromium etcher. By this process, a grating formed by successive rough and smooth strips of glass is produced. In Fig. 4 a photograph is shown of the manufactured grating acquired with a confocal microscope (SensofarTech's PLμ confocal imaging profiler, Sensofar Tech, Barcelona). Since the rough part of the grating is produced using a chemical attack, the grating levels are not exactly of the same height. Also, the glass etching creates irregularities in the fringe borders.

As illumination source we used a collimated laser beam, which impinged normal to the grating, and the far-field diffraction pattern was observed with a system of lenses and a CMOS camera. To obtain the ensemble of intensity distribution patterns we acquired 200 photographs moving the grating along the x axis between every two photographs. The average of the experimental far-field diffraction patterns is shown in Fig. 5(a). Diffraction orders appear along with the halo produced by the rough strips of the grating. This structure corresponds to the high roughness limit depicted in Eq. (18). The halos produced at the different diffraction orders are so wide that

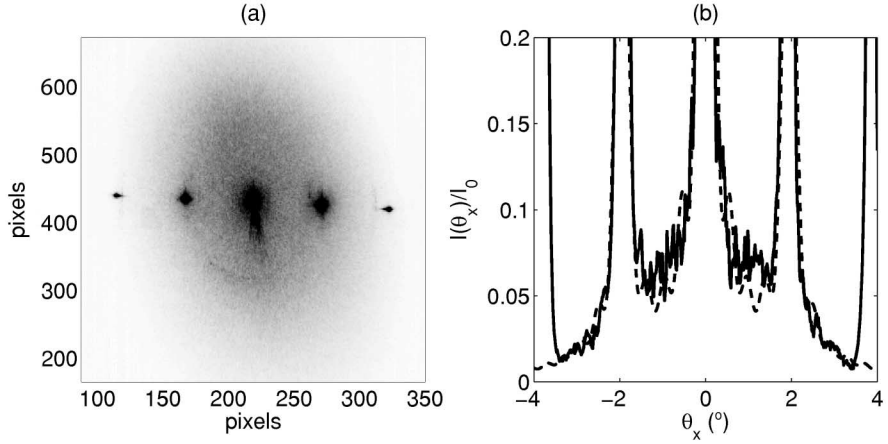

Fig. 5. (a) Average of an ensemble of experimental diffraction patterns of the grating, showing the different diffraction orders and the halo produced by scattering. In order to see the halo, the integration time of the camera needs to be increased so the pixels at the location of the diffraction peaks are saturated. (b) Theoretical fit (dashed curve) to the experimental diffraction pattern (solid curve).

they overlap. In Fig. 5(b) the profile along the diffraction orders is shown, and it is compared with the theoretical model.

The roughness parameters to include in the theoretical model are obtained from the confocal microscope image. These parameters yielded $T_0=51$ μm and $\sigma=0.5$ μm. As shown in Fig. 5(b), the theoretical and experimental mean intensity distributions at $\theta_y=0$ present a similar structure, except for the even diffraction orders. This effect is not predicted with our approach. In any case, the rest of the diffraction pattern fits perfectly, as is evident in Fig. 5(b). The fact of a different average height for the grating levels is not important for the high-roughness grating since, as we have explained before, smooth levels act as an amplitude grating, and high roughness scatters light in all directions.

We think that the apparition of the even orders is due to the irregular shape of the edges, since the grating is not symmetrical. This can be shown by binarizing Fig. 4 into two levels (0 and 1) and numerically determining the far-field diffraction pattern. Then, even orders are obtained, which is a consequence only of the edges, not of the topography. The effect of these irregularities in the edges is totally different from the effect of surface roughness. Surface roughness produces diffraction orders that are surrounded by a "halo." On the contrary, as we have pointed out, the irregularities in the edges of the slits produce even diffraction orders. In any case, this effect means that our experimental results are preliminary, since we should have well-defined edges. The combined theoretical formalism, including the roughness topography and the irregularities in the edges, is too complicated to be solved analytically.

5. CONCLUSIONS

In this work, a diffraction grating formed by a periodic arrangement of strips with two different roughness levels is analyzed. The rough strips produce a random modulation of the phase of the incident light beam. Statistical techniques are required to obtain the mean intensity distribution at the far field. The efficiency and shape of the diffraction orders are shown to depend on the roughness parameters of the grating strips. For high roughness levels the shape of the diffraction orders follows the well-known $\mathrm{sinc}^2(x)$ structure along with a wider intensity distribution around the diffraction orders produced by a scattering process. For the low roughness approach, the diffraction orders present a Lorentz profile. Preliminary experimental results are obtained that corroborate the theoretical model presented. However, the fabrication technique produced irregularities in the edges of the slits and as a consequence, we experimentally obtain even orders that are not predicted by our model of grating with rough surface.

ACKNOWLEDGMENTS

The authors thank A. Luis, F. Perez-Quintian, and J.M. Rico-Garcia for their fruitful ideas and discussions. This work has been supported by the DPI2005-02860 project of the Ministerio de Educación y Ciencia of Spain and a CENIT project "Tecnologías avanzadas para los equipos y procesos de fabricación de 2015: e-eficiente, e-cológica, e-máquina (eEe)" of the Ministerio de Industria, Turismo y Comercio. During the realization of this work Sanchez-Brea was contracted under the "Ramón y Cajal" research program of the Ministerio de Educación y Ciencia of Spain.

REFERENCES

1. M. Born and E. Wolf, *Principles of Optics* (Pergamon, 1980).
2. J. W. Goodman, *Introduction to Fourier Optics* (McGraw-Hill, 1968).
3. E. G. Loewen and E. Popov, *Diffraction Gratings and Applications* (Marcel Dekker, 1997).
4. M. J. Lockyear, A. P. Hibbins, K. R. White, and J. R. Sambles, "One-way diffraction grating," Phys. Rev. E **74**, 056611 (2006).
5. S. Wise, V. Quetschke, A. J. Deshpande, G. Mueller, D. H. Reitze, D. B. Tanner, and B. F. Whiting, "Phase effect in the diffraction of light: beyond the grating equation," Phys. Rev. Lett. **95**, 013901 (2005).
6. C. Palmer, *Diffraction Grating Handbook* (Richardson Grating Laboratory, New York, 2000).
7. R. Petit, *Electromagnetic Theory of Gratings* (Springer-Verlag, 1980).
8. F. Gori, "Measuring Stokes parameters by means of a polarization grating," Opt. Lett. **24**, 584–586 (1999).
9. C. G. Someda, "Far field of polarization gratings," Opt. Lett. **24**, 1657–1659 (1999).
10. G. Piquero, R. Borghi, A. Mondello, and M. Santarsiero, "Far field of beams generated by quasi-homogeneous sources passing through polarization gratings," Opt. Commun. **195**, 339–350 (2001).
11. F. J. Torcal-Milla, L. M. Sanchez-Brea, and E. Bernabeu, "Talbot effect with rough reflection gratings," Appl. Opt. **46**, 3668–3673 (2007).
12. L. M. Sanchez-Brea, F. J. Torcal-Milla, and E. Bernabeu, "Talbot effect in metallic gratings under Gaussian illumination," Opt. Commun. **278**, 23–27 (2007).
13. B. E. A. Saleh and M. C. Teich, *Fundamentals of Photonics* (Wiley, 1991).
14. P. Beckmann and A. Spizzichino, *The Scattering of Electromagnetic Waves from Rough Surfaces* (Artech House Norwood, 1987).
15. J. W. Goodman, *Statistical Optics* (Wiley, 1985).